JOURNAL OF MATERIALS SCIENCE 26 (1991) 2329–2336

Study on powder properties of Fe–P–C and Fe–B–Si alloy powders prepared by water atomization

TAKASHI SATO
Nikkin R & D Co., Ltd. 4-10-1, Funato, Itabashi-ku, Tokyo 174, Japan

The glass-forming region, microstructure and powder properties of iron-based ternary alloy powders prepared by water atomization have been studied. It was observed that the intermetallic compound and the α-phase exist in the hyper-eutectic region and in the hypo-eutectic region, respectively, as a main crystalline phase. No flowability was observed for the powders in the glass-forming region, that is, for amorphous powders. Further, it was found that irregularity in shape and the mean diameter increase and the apparent density decreases as the eutectic composition is approached.

1. Introduction

Previous investigations of amorphous alloy powders have been focused mainly on the production method and the properties of individual powders [1–6]. Up to now systematic study on the amorphous powders has not been performed. This is probably because the powders produced by a number of rapid solidification techniques [6] undergo the gradual transition with increasing particle size from amorphous to equilibrium. As a manufacturing process of amorphous alloy powders, the author presented a new process [7] which is a modified water atomization process. The powders prepared by this process do not undergo a gradual transition from amorphous to equilibrium with increasing particle size, because the powders are fibre-like or spherical when they are small and thin irregularly shaped when coarse.

For the water atomization process, it is well known that the powder properties are influenced to a large extent by physical properties such as surface tension and viscosity of the liquid metal and by the process parameters such as water jet velocity, flow rate of water etc. We cannot, however, predict the powder properties from these properties and parameters.

To utilize the powder metallurgy techniques for practical applications, the knowledge of the powder properties relating to one is extremely important. This report describes the result of the investigations of the glass-forming region, the identification of the crystalline phase and the powder properties for Fe–P–C and Fe–B–Si ternary alloy powders prepared by the rapid quenching water atomization process (RQWAP).

2. Experimental procedure

Alloy powders of $Fe_xP_yC_z$ and $Fe_xB_ySi_z$, where $x = 70$ to 85, $y = 1$ to 24, $z = 0$ to 19 at%, were prepared by rapid quenching water atomization. Commercial electrolytic iron, ferro-phosphorus, ferro-boron, metallic silicon and vacuum-melted high carbon iron mother alloy were used as raw materials. The water atomization was performed at a pressure of 12 MPa and a flow rate of 16.2 $m^3 h^{-1}$. The molten metal stream flowed from an orifice of 3 mm diameter at 1673 or 1723 K. The powders were dehydrated rapidly and then dried under air.

The glass-forming region was determined by use of X-ray diffraction (XRD), differential thermal analysis (DTA) and a vibrating sample magnetometor (VSM). The crystalline phases were analysed by X-ray diffraction using a MoKα radiation in the range of 2θ between 16° and 50°. The crystallization temperature and the liquidus temperature were determined by use of DTA at a heating rate of 10 K min^{-1}. Further, the magnetization of powders was measured by use of a VSM at room temperature. The saturation magnetization was determined by plot of $1/H^2$ against σ. The microstructure of the powders was observed using an optical microscope after the powders were first polished and then etched with 5% nital or picral.

The particle size distribution, apparent density, transverse rupture strength, microhardness, green density etc. were measured for − 100 mesh powders. A mechanical sieve shaker combining rotary motion and tapping action was employed to evaluate the particle distribution. The tapping time was 15 min. The apparent density and the flowability were measured in accordance with JIS Z2504 and JIS Z2502, respectively. The transverse rutpure strength was also determined in accordance with ASTM Designation B 312-58T. These specimens were compacted at a pressure of 700 MPa. The green density was measured on a ring specimen with an outside diameter of 35 mm, an inside diameter of 25 mm and a height of 4 mm. The compacting pressure was 0.5 to 2.5 GPa. The hardness was measured using a Vickers micro-hardness tester at a load of 25 g.

0022–2461/91 $03.00 + .12

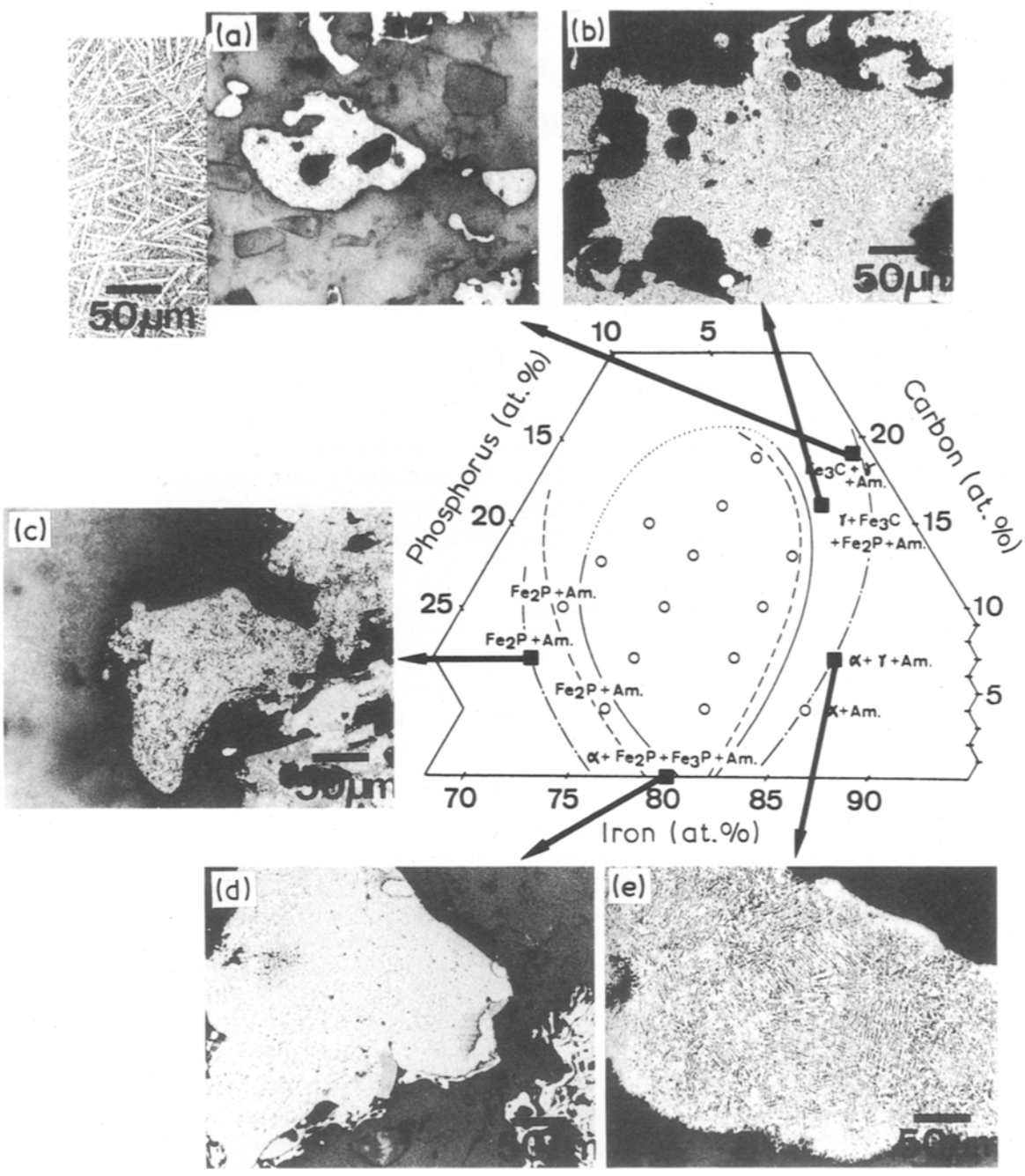

Figure 1 Glass-forming region and microstructures for Fe–P–C powders: (——) powders, determined by XRD; (- - -) ribbons 30 μm thick, extrapolated from results reported by Inoue *et al.* [8]; (– · –) powders, determined by DTA; Am., amorphous.

3. Results and discussion

3.1 Effect of composition on glass-forming region and microstructure

Fig. 1 shows the glass-forming region and the microstructure of the Fe–P–C powders less than 100 mesh. The solid line indicates the glass-forming region which was determined by XRD. The as-prepared powders in this region are completely amorphous as far as we can observe by XRD. In Fig. 1, the broken line indicates the glass-forming region for ribbons with a thickness of 30 μm, which was extrapolated from the data reported by Inoue *et al.* [8]. There is a small difference between the two results. The cooling rate of the powders prepared by RQWAP can be calculated from a mean diameter of the powder [9]. A rough estimate of the cooling rate of a particle of 30 μm is about 10^6 K s^{-1}. This value is nearly equal to the cooling rate of a single-roller technique. The mean diameters at the neighbourhood of the boundary of the glass-forming region for iron-rich and phosphorus-rich powders are about 30 and 50 μm, respectively. Therefore, these small differences are probably caused by a difference of the thickness between the particles and the ribbons. The glass-forming region determined by DTA, moreover, is shown in Fig. 1 with a broken line. The phase mixtures of crystalline and amorphous were observed in the region between the solid and broken curves.

At the iron–rich region in Fig. 1, the precipitated phase is only α-phase in the case of low carbon content. The lattice constant of the α-phase is slightly smaller than that for pure iron. With increasing carbon content, the γ-phase and Fe_3C were observed in the place of the α-phase, and a small amount of Fe_2P and

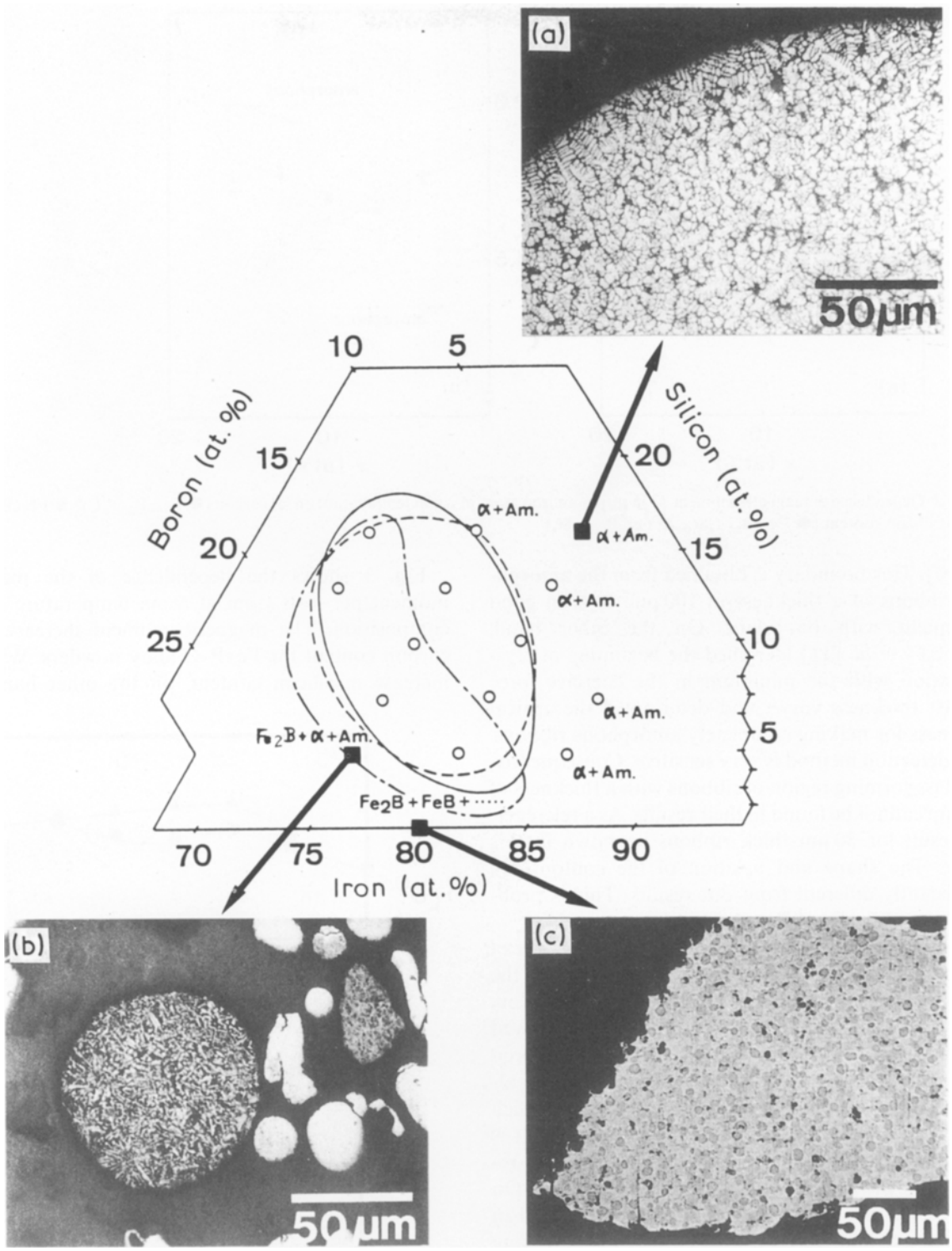

Figure 2 Glass-forming region and microstructures for Fe–B–Si powders: (——) powders, determined by XRD; (- - -) ribbons 100 μm thick, extrapolated from results reported by Hagiwara *et al.* [10]; (–·–) ribbons 30 μm thick, reported by Luborsky *et al.* [11]; Am., amorphous.

α-phase as well in a 16 at %C–4 at %P powder. It is well known that the freezing hypo-eutectic Fe–C alloy involves first the formation of primary dendrite of austenite, followed by the solidification of the eutectic of cementite and austenite. The primary crystal of the alloy containing 2.5 to 17.5 at % C is austenite. The precipitated crystalline phase of 4 at % C powder is, however, only α-phase. This may be caused by the extension of δ + liquid field as a result of being alloyed with phosphorus. Further, it is known that the Fe–P alloy is easily supercooled by rapid quenching, followed by the formation of a metastable (α + Fe_2P) eutectic, therefore, it is thought that Fe_2P and α-phase were observed in a 16 at % C powder. Although the microstructure of the low phosphorus and high carbon powder is probably cementite, that of other powders is dendrite.

In Fig. 2, the mean diameter of powders in the neighbourhood of the boundary of the glass-forming region is about 50 μm for boron-rich powders, while that of other powders in the neighbourhood of the boundary are about 100 μm. The broken curve indicates the glass-forming region of ribbons, which was extrapolated from the data reported by Hagiwara *et*

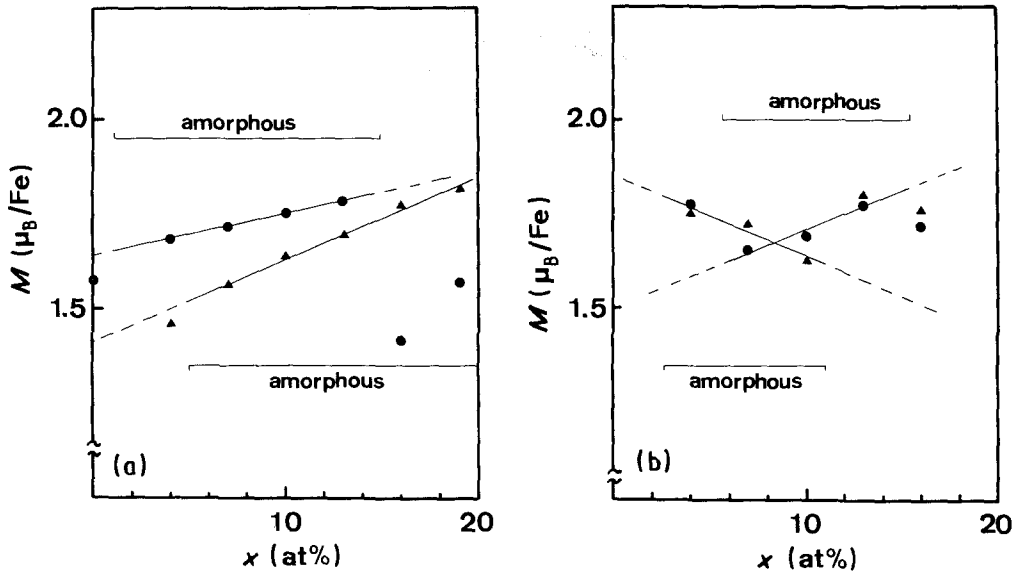

Figure 3 Dependence of magnetic moment $\bar{M}$ in μ_B per an iron atom at room temperature on (a) carbon (● $Fe_{80}P_{20-x}Cx$, ▲ $Fe_{75}P_{25-x}C_x$) and (b) silicon content (● $Fe_{75}B_{25-x}Si_x$, ▲ $Fe_{80}B_{20-x}Si_x$).

al. [10]. This boundary is obtained from the amorphous ribbons of a thickness of 100 μm. It is in good agreement with our data. On the other hand, Luborsky *et al.* [11] identified the beginning of crystallization with the minimum in the coercive force against thickness curve, and determined the critical thickness for making completely amorphous ribbons. This detection method is very sensitive. Consequently, the glass-forming region of ribbons with a thickness of 100 μm cannot be found in their results. As a reference, the result for 30 μm thick ribbons is shown in this figure. The shape and position of the contour are significantly different from our results. This is probably caused by the different detection method.

The precipitated crystalline phase in the region of low carbon content is only an α-phase of which the lattice constant is smaller than that of pure iron. Silicon, with a favorable size factor, is readily alloyed with iron, and occupies substitutional sites. The boron atom probably also occupies substitutional sites, although the atomic radius is nearing the stage at which an interstitial solid solution would be preferred. It is thought, therefore, that the small lattice constant results from the arrangement of silicon and boron. On the other hand, α-phase and Fe_2B were observed in the region of high boron content. The X-ray scattering intensity of these phases is nearly the same. The precipitated crystal of an Fe–B binary alloy powder is Fe_2B and FeB, the scattering intensities of which are nearly equal.

As for the powder including crystalline phase, it can be seen from these results that α-phase in the hypo-eutectic region and intermetallic compound in the hyper-eutectic region exist as a main crystal.

If aluminium is added or contained in liquid metal, a very narrow glass-forming region is formed. Further, the presence of aluminium interferes with the stream of liquid metal through the orifice, and finally stops it. In order to prevent it, the temperature of the liquid metal must be raised. The rise in temperature, however, is undesirable for the prevention of the oxidation of the particles.

Fig. 3 shows the dependence of the magnetic moment per iron atom at room temperature on the composition. The magnetic moment increases with carbon content for Fe–P–C alloy powders. With the increase in silicon content, on the other hand, the

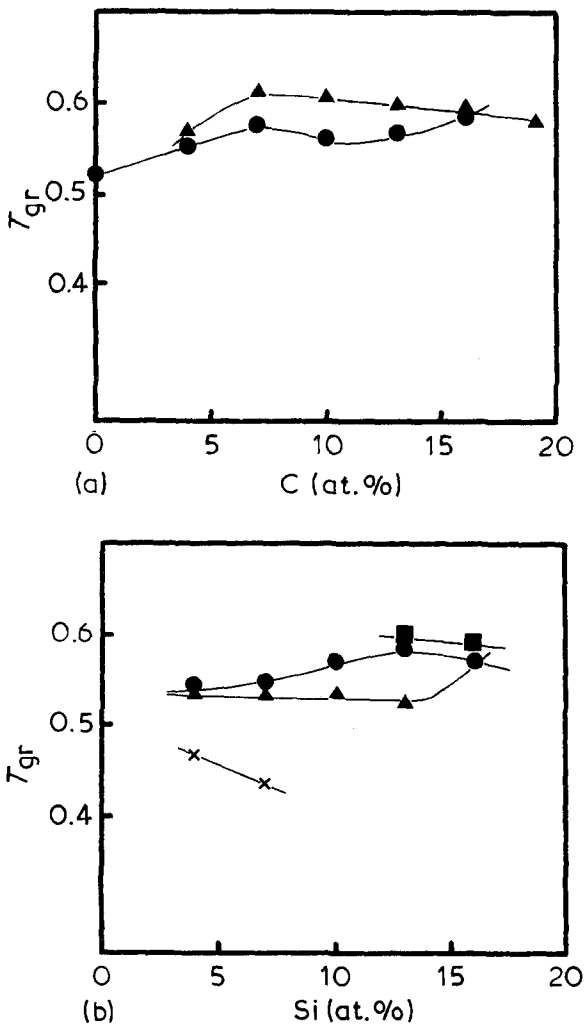

Figure 4 Variation of the reduced glass temperature Tgr for glass formation with metalloid content for (a) Fe–P–C system (▲ 75 at % Fe, ● 80 at % Fe) and (b) Fe–B–Si system (■ 70 at %Fe, ● 75 at % Fe, ▲ 80 at % Fe, ×, 85 at %Fe).

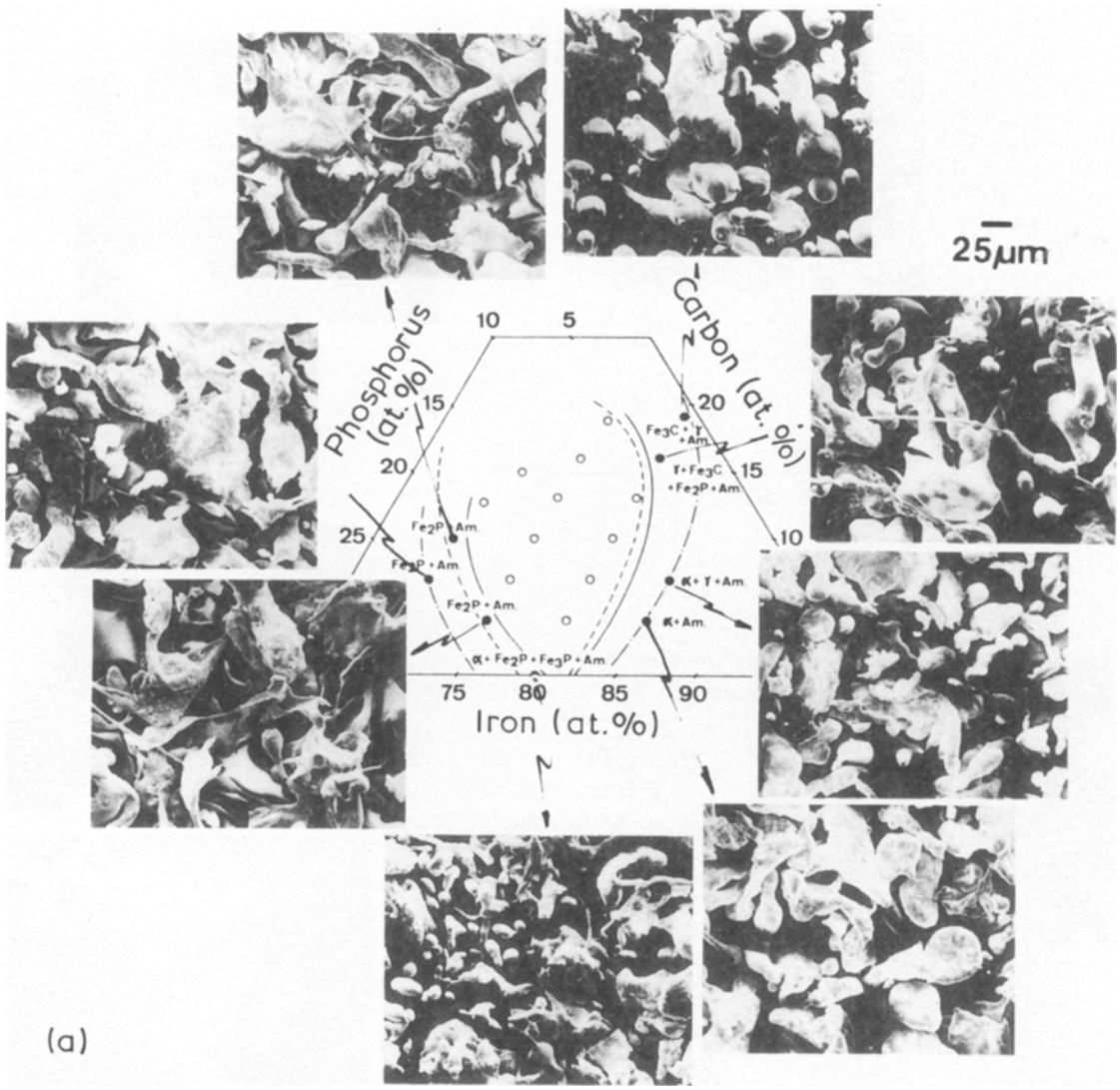

Figure 5 Scanning electron micrographs of powders at the neighbourhood of the boundary of the glass-forming region for (a) Fe–P–C and (b) Fe–B–Si system.

magnetic moment of $Fe_{75}B_{25-x}Si_x$ powders increases and that of $Fe_{80}B_{20-x}Si_x$ powders decreases. The data for 80 at % Fe are different from the previous study [12]. The magnetic moment of the amorphous powders which included the crystalline phase deviates from the straight line as shown in this figure. It can be seen from this result that the glass-forming region of the powders is exact.

Fig. 4 shows the dependence of $T_x/T_m = T_{gr}$ on the composition where T_x and T_m are crystallization temperature and liquidus temperature, respectively. When T_x is measured dynamically under conditions of relatively rapid heating, it approximates more closely to the glass transition temperature T_g. It is known that the liquidus temperature often decreases around a deep eutectic point. In such cases, the interval between liquidus temperature and T_g generally decreases, so that the probability of being able to cool through the interval without inducing crystallization is enhanced, i.e. the glass forming ability is increased [13]. Although T_{gr} tends to decrease with increasing iron content for both Fe–P–C and Fe–B–Si systems the value of T_{gr} on which the amorphous phase must be formed could not be determined from the results in Fig. 3.

3.2 Effect of composition on powder properties

The processing of a powder into a compact and the resultant properties of P/M parts are affected by such physical characteristics as particle size, particle size distribution, particle shape and microstructure, and surface condition. Other characteristics, such as apparent density and flowability depend on these basic physical properties. Relationships between these powder properties and their behaviour during processing in most cases are qualitative in nature. Nevertheless, a good description of powder properties is important.

Fig. 5 shows scanning electron micrographs of the powders which lie in the neighbourhood of the boundary line of the glass-forming region. The shape of these powders is rather spherical and smooth, although that of the powders which have eutectic composition is very irregular. The disintegration and deformation of a liquid droplet are determined by the following relation

$$P \gtrapprox F(\gamma) + F(\mu) + F^* \quad (1)$$

where, P, $F(\gamma)$, $F(\mu)$ and F^* are the dynamic pressure [14], the surface tension, the force resulting from viscosity and the thermo–chemical reaction [15], re-

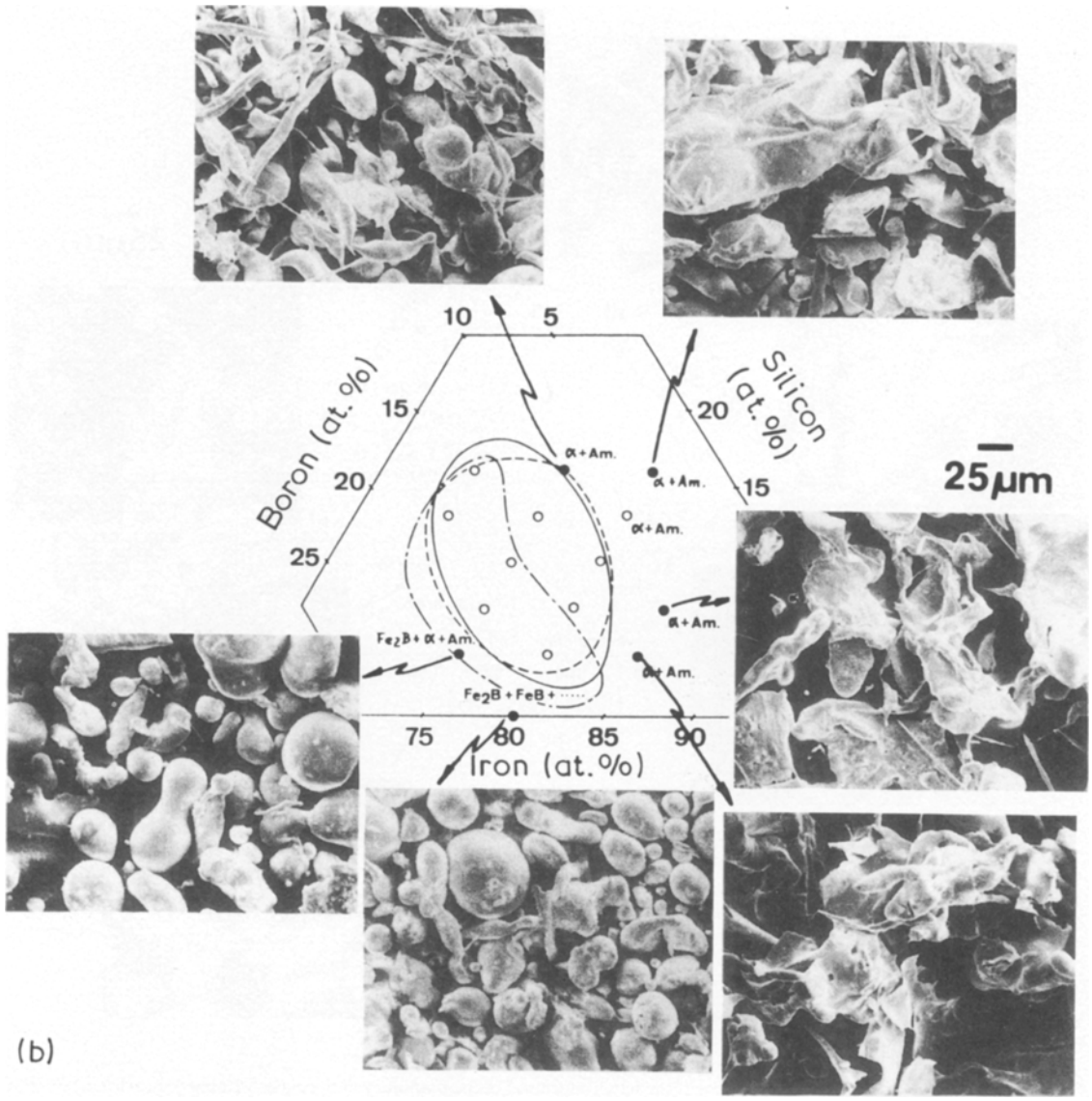

Figure 5 Continued

spectively. If the particle was rapidly cooled, the thermo–chemical reaction can be neglected. Liquid metal with eutectic composition have high viscosity, and $F(\mu)$ is enhanced, the probability of secondary disintegration decreases. Therefore, irregular and large particles are solidified. On the other hand, if the composition is very far apart from eutectic composition, the viscosity becomes small. Thus, the secondary disintegration is determined by $F(\gamma)$ and dynamic pressure P. If $F(\gamma)$ becomes larger than dynamic pressure P, the disintegration stops, and small and rather spherical powders are produced. The force which acts on the droplets is given by

$$F \simeq 4F(\gamma)/d \qquad (2)$$

that is to say, the shape of powders becomes more spherical as the particle size decreases.

Fig. 6 shows the particle size distribution. The curve shifts to the large mean diameter with increase in viscosity of both Fe–P–C and Fe–B–Si systems. As a reference, the data of SUS304L powders are also shown in this figure.

The dependence of the mean diameter, the apparent density, the transverse rupture strength and the green density on the composition are shown in Fig. 7. The compositional dependence of the apparent density and of the mean diameter displays the reverse behaviour, and the value of the apparent density is much smaller than that of metal powders which are used for powder metallurgy. It is thought that the apparent density of the amorphous powders prepared by RQWAP were affected especially by particle shape, surface roughness of individual particles and particle arrangement. The apparent density reduces as the surface roughness increases and the shape of powders becomes less spherical, due to both the increase in frictional surface area and the lower uniformity of powder particles during packing. That is to say, the packing structure of particles is affected by the interaction between settling particles. If the interaction between settling particles is smaller than their momentum, the particles form a close packed structure, however, if the interaction between the particles becomes more intense, the free spaces between previous settled particles increase, thereby the apparent density decreases. The apparent densities of Fe–P–C powders are relatively high compared with those of Fe–B–Si powders. This is probably caused by the

difference of surface oxide films rather than the particle shape.

Flow rate is one of the important properties of a powder. It is most strongly affected by interparticle friction, that is, interaction between particles. The flow rate of the amorphous powders prepared by RQWAP was measured, but it could not be observed because of their remarkably irregular shape. Some compacting tools require a free-flowing powder, while others can be used with a relatively poor-flowing powder. It is found, therefore, that these amorphous powders must be granulated in preference to the die-filling operation of a production press.

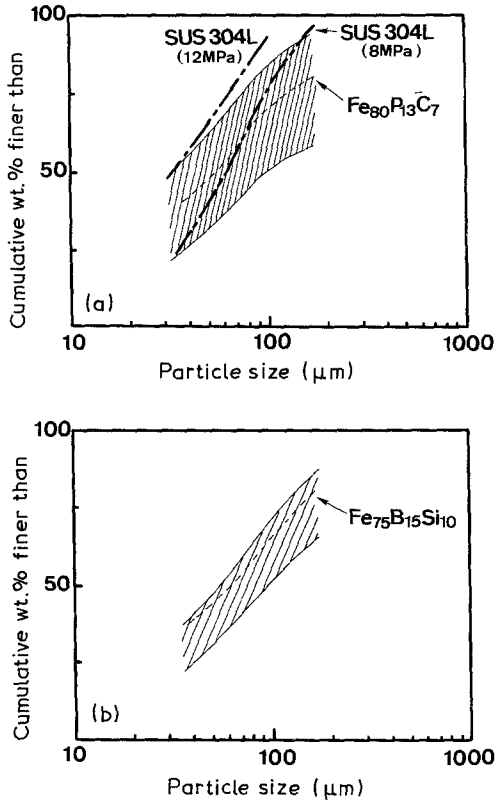

Figure 6 Cumulative plot of particle size distributions of a rapid quenching water atomized (a) Fe–P–C and (b) Fe–B–Si alloy powders.

In general, since considerable deformation of a powder takes place during pressing, its work-hardening characteristics have a strong influence on compressibility. The green density of the amorphous powders increased linearly with the compacting pressure within the pressure of 0.5 to 2.5 GPa. It is almost, however, independent of the composition as shown in this figure, and the value of the green density of the powders compressed at 2.5 GPa is merely 85 TD%. The amorphous alloy is nevertheless a perfectly plastic solid, it is a non-strain-hardening material which possesses large inelasticity and high strength and hardness, that is to say, poor compressibility is probably caused by mechanical properties of amorphous alloy.

On the other hand, the transverse rupture strength depends on the composition, and its behaviour is similar to that of the mean diameter. Namely, the transverse rupture strength increases with increasing irregularity in shape. The maximum value of the transverse rupture strength corresponds approximately to that of the stainless steel powder compacted at 0.7 GPa. Transverse rupture strength of green compacts results mainly from mechanical interlocking of irregularities on the particle surfaces, which is promoted by plastic deformation during pressing. Particle shape is, therefore, the most important factor contri-

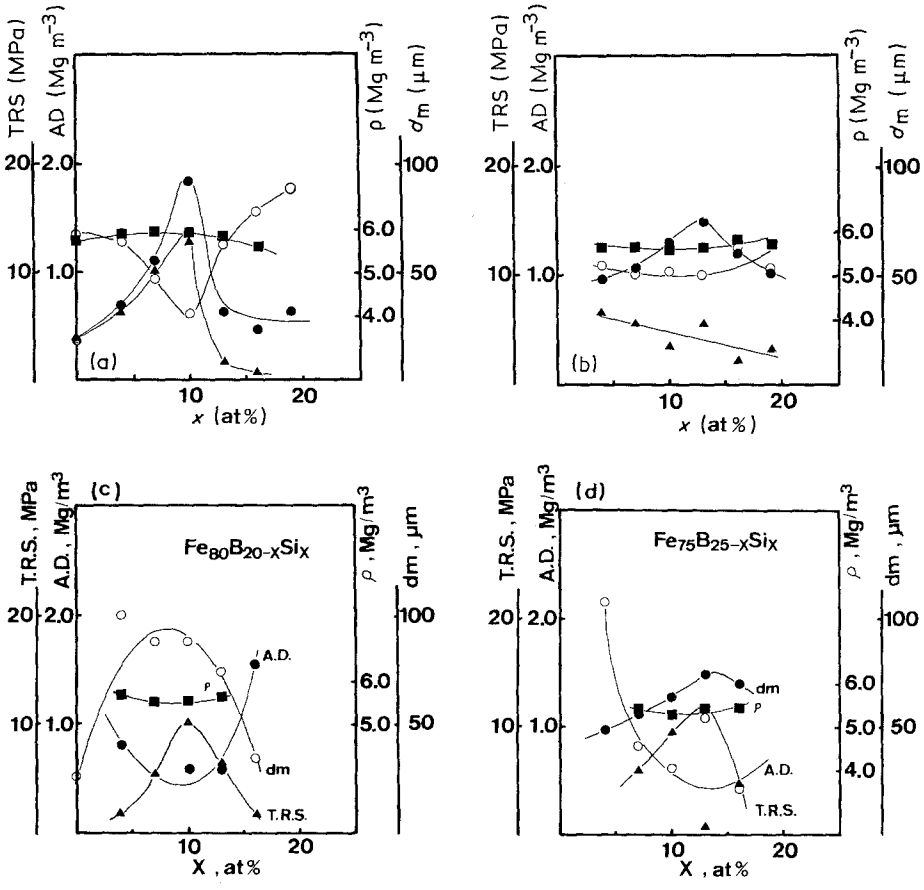

Figure 7 Variation of mean diameter (d_m) (●), apparent density (A.D.) (○), transverse rupture strength (T.R.S.) (▲) and green density (ρ) (■) for (a)(b) Fe–P–C and (c)(d) Fe–B–Si systems.

buting to transverse rupture strength. It is also increased when oxidation and contamination of particle surfaces are reduced.

4. Conclusions

Fe–P–C and Fe–B–Si alloy powders were prepared by rapid quenching water atomization, and the glass-forming region, the microstructure and the powder properties were investigated. The results are as follows:

(1) The glass-forming region of the alloy powders is nearly equal to that of amorphous ribbons prepared by the single-roller technique.

(2) As to the powder induced crystalline phase, α-phase and intermetallic compound exist in the hypo-eutectic region and the hyper-eutectic region, respectively, as a main crystal.

(3) $T_{gr}(= T_x/T_m)$ decreases with increasing iron content for both Fe–P–C and Fe–B–Si systems.

(4) With the approach to eutectic composition, irregularity in shape and the mean diameter increase and the apparent density decreases.

(5) No flowability was observed for powders in the glass-forming region, that is, for amorphous powders.

(6) The green density of the amorphous powders is independent of the composition.

Acknowledgment

The author would like to thank T. Nakagawa and R. Sakai for carrying out some experiments.

References

1. A. E. BERKOWITZ and J. L. WALTER, *Mater. Sci. Eng.* **55** (1982) 275.
2. R. J. PATTERSON, D. L. LEDWITH and J. C. DWYER, in "Processing metallic ceramic powders", edited by R. M. German and K. W. Lay (The Metallurgical Society of AIME, Kentucky, 1982) p. 33.
3. A. E. BERKOWITZ, J. C. GRANDE, S. A. MILLER, R. J. MURPHY and J. L. WALTER, *Mater. Sci. Eng.* **62** (1984) 217.
4. H. YASHITA, M. YOSHIKAWA, T. FUNABIKI, S. YOSHIDA and Y. ISOZUMI, *J. Mater. Sci. Lett.* **5** (1986) 1163.
5. J. L. WALTER and A. E. BERKOWITZ, in "Science and technology of rapidly quenched alloys", edited by M. Tenhover, W. L. Johnson and L. E. Tanner (Materials Research Society, Pennsylvania, 1987) p. 179.
6. S. A. MILLER, in "Amorphous metallic alloys", edited by F. E. Luborsky (Butterworth, London, 1983) p. 506.
7. T. SATO, *Scripta Metall.* **20** (1986) 1801.
8. A. INOUE, M. HAGIWARA and T. MASUMOTO, *J. Mater. Sci.* **17** (1982) 580.
9. T. SATO, *J. Mater. Sci. Lett.* **6** (1987) 844.
10. M. HAGIWARA, A. INOUE and T. MASUMOTO, *Sci. Rep. RITU* **A29** (1981) 351.
11. F. E. LUBORSKY, J. REEVE, H. A. DAVIES and H. H. LIEBERMAN, *IEEE Trans. Magnetics* **MAG-18** (1982) 1385.
12. N. S. KAZAMA, M. MITERA and T. MASUMOTO, in "Rapidly quenched metals III" edited by B. Cantor (The Metals Society, London, 1978) p. 164.
13. H. A. DAVIES, in "Amorphous metallic alloys", edited by F. E. Luborsky (Butterworth, London, 1983) p. 8.
14. K. TAMURA and S. WANIKAWA, *J. Jpn. Soc. Powder & Powder Metall.* **15** (1968) 302.
15. J. J. DUNKLEY, *Chem. Ind. N Z* **13** (1979) 15.

Received 9 October
and accepted 24 October 1989